



Published in final edited form as:

J Phys Chem B. 2012 June 7; 116(22): 6387–6396. doi:10.1021/jp303303v.

Nitroxide Sensing of a DNA Microenvironment: Mechanistic Insights from EPR Spectroscopy and Molecular Dynamics Simulations

Anna M. Popova^{1, #, †}, Ma'mon M. Hatmal^{2, #}, Maria Frushicheva¹, Eric A. Price^{3, ‡}, Peter Z. Qin^{1, *}, and Ian S. Haworth^{2, 4, *}

¹Department of Chemistry, University of Southern California, Los Angeles, California 90089-0744

²Department of Biochemistry, University of Southern California, Los Angeles, California 90033-1039

³Department of Biological Sciences, University of Southern California, Los Angeles, California 90089-0744

⁴Department of Pharmacology and Pharmaceutical Sciences, University of Southern California, Los Angeles, California 90089-9121

Abstract

The behavior of the nitroxide spin labels 1-oxy-4-bromo-2,2,5,5-tetramethylpyrroline (R5a) and 1-oxy-2,2,5,5-tetramethylpyrroline (R5) attached at a phosphorothioate-substituted site in a DNA duplex is modulated by the DNA in a site- and stereospecific manner. A better understanding of the mechanisms of R5a/R5 sensing of the DNA microenvironment will enhance our capability to relate information from nitroxide spectra to sequence-dependent properties of DNA. Towards this goal, electron paramagnetic resonance (EPR) spectroscopy and molecular dynamics (MD) simulations were used to investigate R5 and R5a attached as R_p and S_p diastereomers at phosphorothioate $pS C_7$ of d(CTACTG $pS C_7 Y_8$ TTAG). d(CTAAAGCAGTAG) (Y = T or U). X-band continuous-wave EPR spectra revealed that the dT_8 to dU_8 change alters nanosecond rotational motions of R_p -R5a, but produces no detectable differences for S_p -R5a, R_p -R5, and S_p -R5. MD simulations were able to qualitatively account for these spectral variations and provide a plausible physical basis for the R5/R5a behavior. The simulations also revealed a correlation between DNA backbone B_I/B_{II} conformations and R5/R5a rotational diffusion, thus suggesting a direct connection between DNA local backbone dynamics and EPR-detectable R5/R5a motion. These results advance our understanding of how a DNA microenvironment influences nitroxide motion and the observed EPR spectra. This may enable use of R5/R5a for a quantitative description of the sequence-dependent properties of large biologically relevant DNA molecules.

Keywords

DNA; nitroxide; EPR; molecular dynamics; stereospecificity

*To whom correspondence should be addressed: an Haworth: PSC-304B, 1985 Zonal Avenue, Los Angeles, CA 90089-9121; Tel: (323) 442 3310; Fax: (323) 442 1390; ihaworth@usc.edu, Peter Z. Qin: LJS-251, 840 Downey Way, Los Angeles, CA 90089-0744; Tel: (213) 821-2461; Fax: (213) 740-0930; pzq@usc.edu.

#These authors contributed equally to the manuscript

†Current address: Department of Molecular Biology, The Scripps Research Institute, La Jolla, California, 92037

‡Current address: Department of Physiology, University of Arizona, Tucson, Arizona 85724

Supporting Information Available

Tables S1 to S6 and Figures S1 and S2 are provided as supplemental information. This information is available free of charge via the Internet at <http://pubs.acs.org>

Introduction

Physical properties of DNA, such as helix geometry, flexibility, water and ion binding, and electrostatics have a critical impact on biological functions of gene expression and regulation. Sequence-dependent deviations from the ideal B-form in DNA duplexes play essential roles in DNA recognition by proteins and small molecules.¹⁻⁴ For example, DNA sequence-dependent mechanics (i.e., deformability, bending) and local shape variations provide a code to guide nucleosome binding in eukaryotic genomes,⁵⁻⁷ which may modulate the activity of transcription factors and other DNA-binding proteins and profoundly affect gene expression. However, knowledge of the sequence dependence of the structure and flexibility of DNA has yet to reach a level that allows rational design and manipulation of functions.^{2,3} Thus, experimental and computational characterizations of the conformational and dynamic heterogeneity of free DNA duplexes are of significance.^{2,4}

Site-directed spin labeling (SDSL) is a biophysical tool for investigating local environments in bio-macromolecules.⁸⁻¹¹ In SDSL, a chemically stable nitroxide radical is covalently attached at specific sites of a protein, DNA or RNA. The nitroxide behavior, which is revealed by electron paramagnetic resonance (EPR) spectroscopy, provides structural and dynamic information on the parent molecule. SDSL requires a small amount of sample (~50 μM in 5 μl) and can be applied to characterize high molecular weight systems under physiological conditions. In nucleic acid studies, SDSL has been used to deduce the structural state of individual nucleotides, to reveal local motions, and to monitor conformational changes in nucleic acids and protein/nucleic acid complexes.¹¹⁻¹⁷

We have developed a phosphorothioate labeling scheme^{18,19} in which a nitroxide probe (R5 or R5a, Figure 1A) is attached via a flexible R-C-S-P linkage at a R_p or S_p phosphorothioate (Figure 1B) that is chemically substituted at a specific nucleotide in a DNA or RNA strand. R5 and R5a minimally perturb the native duplex conformation of DNA²⁰⁻²² and RNA,^{23,24} and have been used to monitor RNA/RNA interactions,¹⁸ to study motions of an RNA element within a large folded ribozyme,²⁴ and to measure nanometer distances and conformation in nucleic acids.^{20,23,25} We have also shown that X-band continuous-wave (cw) EPR spectra of R5a and R5, which reports on nanosecond rotational motions of the nitroxide pyrroline ring, vary within a DNA duplex in a sequence-dependent and stereospecific fashion.^{21,22} This indicates that R5a and R5 can act as sensors to reveal sequence-dependent properties of DNA duplexes.

To understand how the local DNA environment governs the rotational behavior of R5a/R5 labels, in this work we used a combination of EPR spectroscopy and molecular dynamics (MD) simulations to examine how the labels respond to a DNA sequence change: namely the removal of a methyl group in the major groove of a DNA duplex. The results suggest that specific interactions between the label and DNA bases, which depend on the conformational preferences of the label and DNA backbone, can modulate rotational motions of the label to an extent detectable by cw-EPR spectroscopy. These results are a key step forward in developing R5 and R5a as spectroscopic probes for examining intrinsic sequence-dependent features in biologically relevant DNA molecules.

Materials and Methods

DNA labeling, purification, and diastereomer separation

The DNA duplexes d(CTACTG_{pS}C₇T₈TTAG).d(CTAAAGCAGTAG) and d(CTACTG_{pS}C₇U₈TTAG).d(CTAAAGCAGTAG) (_{pS} = phosphorothioate) were used in the study (Figure 1C). These duplexes are referred to as dT₈ and dU₈, respectively. All DNA

oligonucleotides, including those with a phosphorothioate modification, were synthesized by solid-phase chemical synthesis and obtained from Integrated DNA Technologies (Coralville, IA). R5a or R5 were attached to the phosphorothioate-modified DNA strands following reported protocols.²¹ The labeled DNA oligonucleotides were purified using anion-exchange HPLC,^{21,22,26} which eliminates failed oligonucleotide fragments from DNA synthesis, removes excess spin labels, and separates R_p and S_p phosphorothioate diastereomers. The purities of the labeled R_p and S_p oligonucleotides were determined to be >98% by running anion-exchange HPLC on purified samples.²² Diastereomer configurations were assigned as reported.²⁶ The HPLC fractions containing purified labeled DNA were desalted using a G-25 Sephadex column. Desalted oligonucleotides were lyophilized, suspended in 10-15 μL of water and stored at -20°C . The final concentration of labeled deoxyoligonucleotides was determined by UV absorption at 260 nm.^{21,22}

EPR spectroscopy

Spin-labeled DNA oligonucleotides were assembled with the complementary strand following a reported protocol.^{21,22} The final EPR sample ($\sim 10\text{-}15\ \mu\text{L}$) contained 100 mM NaCl, 50 mM Tris-HCl (pH=7.5), 34% (w/w) sucrose, and 20-40 μM labeled DNA duplex. EPR samples were placed in glass capillaries (1.0 mm I.D. \times 1.2 mm O.D., Vitrocom, Inc. Mountain Lakes, NJ) that were sealed on one end. cw-EPR spectra were acquired on a X-band Bruker EMX spectrometer equipped with a high-sensitivity cavity (ER 4119HS, Bruker Biospin, Inc., Billerica, MA) using a 2 mW incident microwave power and field modulation of 1-2 G at 100 kHz. Sample temperature was maintained at 25°C using a liquid nitrogen variable temperature control setup. All EPR spectra were baseline corrected and normalized to the same number of spins using software kindly provided by the Hubbell group at UCLA. In some cases EPR spectra revealed features from a residual amount of a detached spin probe (< 3%). These features were manually subtracted from the reported spectra.^{21,22}

EPR spectra fitting

Spectral fitting was carried out as previously described²² using a MATLAB-based EPRLL program suite²⁷ that implements the Microscopic Order Macroscopic Disorder (MOMD) model.²⁸ The \mathbf{g} and \mathbf{A} tensor, the diffusion tilt angle, the number of director orientations, and dimensions of the basis set were fixed at previously reported values.²² Variable fitting parameters (Supplemental Table S1) included: $\bar{R}(i)$ and N , spherical components of the rotational $\bar{R} = \sqrt{3} \sqrt{R_{\perp}^2 \cdot R_{\parallel}}$ diffusion rate tensor (and $N = R_{\parallel}/R_{\perp}$, where R_{\parallel} and R_{\perp} are the respective rate constants for rotations parallel and perpendicular to the nitroxide principal diffusion axis); (ii) c_{20} , the coefficient of an ordering potential

($U(\theta) = -\frac{1}{2}(k_b T) \cdot c_{20} \cdot (3\cos^2\theta - 1)$, where θ is an instantaneous angle relating the director to the nitroxide diffusion frame); and (iii) $\Delta^{(0)}$, the Gaussian inhomogeneous broadening factor. From the ordering potential, an order parameter, S_{20} , was computed as

$$S_{20} = \left\langle \frac{3\cos^2\theta - 1}{2} \right\rangle = \frac{\int \frac{1}{2}(3\cos^2\theta - 1) \cdot \exp(-U(\theta)/k_b T) \cdot \sin(\theta) d\theta}{\int \exp(-U(\theta)/k_b T) \cdot \sin(\theta) d\theta}$$

Errors for the fitting parameters were obtained as previously described.²²

Structure building for molecular dynamics simulations

Input structures for the molecular dynamics simulations were built from the NMR structure of the dT₈ duplex (model 1 of 1CS2.PDB),²⁹ with either R5a or R5 added using the NASNOX algorithm.^{19,30} In this procedure, a non-bridging oxygen atom of the phosphodiester of nucleotide 7 (OA and OB for the S_p and R_p diastereoisomers,

respectively) was substituted by a sulfur atom with a P-S bond of 1.99 Å, but otherwise the experimental geometry of the duplex was retained. Eight structures were built for each combination of label (R5 or R5a), chirality (R_p or S_p) and DNA sequence (dT₈ or dU₈) with the label conformation set at $t_1=t_2=t_3=180^\circ$ (see Figure 1A for the definition of torsional angles t_1 , t_2 and t_3). Two more sets of eight structures each were built with starting conformations of $t_1=60^\circ$ (S_p) or -60° (R_p), $t_2=180^\circ$, $t_3=0^\circ$; and $t_1=60^\circ$ (S_p) or -60° (R_p), $t_2=180^\circ$, $t_3=120^\circ$. Overall, 24 structures were used as starting points for molecular dynamics simulations of 10 ns each. Based on the results of these simulations, a fourth set with $t_1=180^\circ$, $t_2=120^\circ$, $t_3=180^\circ$ was used for additional simulation of selected combinations of the chirality, label and DNA sequence.

Parameters for the 1-oxyl-4-bromo-2,2,5,5-tetramethylpyrroline (R5a) label

A previously defined geometry for the R5 label³⁰ was maintained for R5a, and the Br atom was added to position 4 of the pyrroline ring with a bond length of 1.94 Å (see Figure 1A for atom nomenclature). Further parameterizations were based on those for the “br” atom type in the General AMBER ForceField (GAFF):³¹ CX-br bond $k_{str} = 269.6$ kcal/(mol·Å²), $r_{eq} = 1.897$ Å (based on GAFF CA-br); CX-CX-br and CY-CX-br angles $k_\theta = 63.0$ kcal/(mol·rad²), $\theta_0 = 123.55^\circ$ (force constant from GAFF, geometry from Price et al.³⁰). Atomic point charges (mE) for the R5a label were P +601; O5' -327; O3' -327; O -344; S -129; CS (HS) +33 (+57); C2 +58; C3 -54; N1 +84; C4 +34; Br -87; C5 +74; O1 -345; C2-Me (H-Me) -88 (+46); C5-Me (H-Me) -83 (+46).

Molecular dynamics simulations

Each labeled duplex was solvated in a periodic box of TIP3P water molecules with the box extending 12 Å from the extremes of the solute in the $\pm x$, $\pm y$ and $\pm z$ directions. This gave a box of approximate dimensions $60 \times 60 \times 75$ Å that contained 6000 to 6500 water molecules (the exact number depended on the starting structure for the simulation). The labeled duplexes were neutralized by addition of 21 sodium ions and the system was minimized for 1000 steps (500 steps of steepest decent, followed by 500 steps of conjugate gradient minimization). Simulations were run using the AMBER parm99 force field with a time step of 0.002 ps, a residue-based cut-off of 8 Å, and the particle-mesh Ewald method for electrostatic interactions.³² SHAKE was applied to all hydrogen atoms and the target pressure was 1 atm. Equilibration of the solvent molecules was achieved in an initial simulation of 5,000 steps (100 ps) with position restraint of all solute atoms (except for sodium ions) with a force constant of 20 kcal/(mol·Å²), during which the temperature of the system was raised linearly from 0 to 298 K over the first 2,500 steps (50 ps). Following the 100-ps solute-restrained period, the restraint on the solute atoms was removed and a further 100 ps of equilibration was performed at 298 K. This was followed by a 10 ns simulation for data collection, during which structures were collected every 0.1 ps.

Three simulations of 10 ns each were also performed for the unlabeled DNA duplex, starting from PDB ID 1CS2 (model 1) and using an identical solvation and equilibration procedure to that for the labeled duplexes. For the unlabeled helix, the structure after 10 ns was resolvated and subjected to re-equilibration to generate a second 10 ns trajectory. The structure after 20 ns was used similarly as a starting point for the third simulation. Results from all simulations were visualized using WebLab Viewer (Molecular Simulations Inc., San Diego, CA) and geometrical data were obtained using AMBER (PTRAJ) and CURVES 5.2.³³

Results

EPR spectra reveal that the dT₈ to dU₈ change affects rotational motion of R_p-R5a only

In this work, R5a and R5 were attached to nucleotide 7 located at the center of the dT₈ or dU₈ duplex (Figure 1C), and R_p and S_p diastereomers were separated to >98% pure (see Methods). R5a or R5 labeling has been previously shown to minimally perturb the native B-DNA conformation of the dT₈ duplex.²⁰⁻²² The dU₈ duplex, which differs from dT₈ only by a thymine C5-methyl group residing in the DNA major groove, is expected to maintain a B-form conformation with or without R5/R5a attachment. This is indeed the case observed in MD simulations.

Figure 2 shows EPR spectra of R5a and R5 obtained at 25°C. The dT₈ to dU₈ change results in a small but reproducible change in R_p-R5a spectra. The R_p-R5a-dU₈ spectrum has narrower lines compared to that of R_p-R5a-dT₈, indicating an increase in R5a mobility upon removal of the dT₈ C5-methyl group. No detectable spectral differences were observed for S_p-R5a, R_p-R5, and S_p-R5 (Figure 2), which suggests that changing dT₈ to dU₈ has no measurable effect on nanosecond rotations of these probes. We also note that the R_p-R5 spectra are broader than those of S_p-R5 (Figure 2). This is consistent with previously reported R_p-R5a and S_p-R5a behavior,²² which has been attributed to the R_p-diastereomer positioning the nitroxide towards the major groove of the DNA duplex, while the S_p-diastereomer positions the nitroxide towards the solvent.

To further characterize rotational motions of R5a, spectral simulations were carried out using the Microscopic Order Macroscopic Disorder (MOMD) model, which describes the nitroxide motion within the macromolecular environment as an anisotropic rotational diffusion constricted by an ordering potential.²⁷ Simulations yield two key parameters: (i) \bar{R} , which describes the rate of nitroxide rotational motions; and (ii) S₂₀, which provides a measure of local ordering. The simulations gave best-fit spectra that match the corresponding measured spectra very well (Figure 3A). The dT₈ to dU₈ change was found to increase R_p-R5a mobility, with a faster rate (larger \bar{R}) and lower ordering (smaller S₂₀) obtained for R_p-R5a-dT₈ (Figure 3B). For S_p-R5a, neither rate nor order parameters are affected by the change from dT₈ to dU₈ (Figure 3B). This is in complete agreement with conclusions drawn from direct lineshape comparisons described above.

In summary, EPR spectra reveal that the dT₈ to dU₈ change gives rise to increased mobility for R_p-R5a, but has no detectable effects on S_p-R5a, R_p-R5, and S_p-R5. These observations are accounted for by MD simulations described below.

MD simulations qualitatively capture observed features of nitroxide rotational behavior in response to the dT₈ to dU₈ change

A total of 40 simulations of 10 ns each were performed in explicit solvent using AMBER on the dT₈ and dU₈ duplexes carrying R5a or R5 as the R_p or S_p phosphorothioate diastereomer of nucleotide 7 (Figure 1). For each sample set, defined by diastereomer configuration (R_p or S_p), label identity (R5a or R5), and DNA sequence (dT₈ or dU₈), the results were obtained by analyzing multiple simulations that differed only in the starting conformation of the label, defined by torsion angles t1 (O5'-P-S-C_s), t2 (P-S-C_s-C₃), and t3 (S-C_s-C₃-C₂) around bonds connecting the nitroxide pyrroline ring to the DNA (Figure 1A). Details of the simulations are reported in Tables S2 and S3 for R_p and S_p labels, respectively. In each simulation, the energy of the system was stable, and the DNA duplex structure was retained, as confirmed by analysis of helical parameters and base pair hydrogen bonds (data not shown).

Variations of the t_1 , t_2 and t_3 torsion angles reflect rotational motions of the nitroxide with respect to the DNA, which is measured by the cw-EPR spectra described above. Torsion angle distributions from all simulations are summarized in Table 1 (see also Tables S2 and S3). For the R_p labels, the MD data show that the dT_8 to dU_8 change yields significant changes only for R_p -R5a, with occupancy of the t_1 *gauche+* (g^+) conformer being $46.6 \pm 24.3\%$ for R_p -R5a- dT_8 vs. $17.7 \pm 9.7\%$ for R_p -R5a- dU_8 (Tables 1 and S2). This suggests that the dT_8 to dU_8 change alters the rotational behavior of R_p -R5a, but has no apparent effect on R_p -R5. This is in agreement with the EPR data (Figures 2 and 3).

For the S_p labels, the sequence change from dT_8 to dU_8 results in no significant changes of all torsion angle distributions except for t_2 in S_p -R5, in which the average occupancy of g^+ and *gauche-* (g^-) conformers differ beyond one standard deviation (Tables 1 and S3). Examination of MD data for S_p labels revealed no discernable nitroxide/DNA interaction that is dependent on the dT_8 to dU_8 change, since the S_p labels are directed away from the DNA helix and into the solvent.^{22,30} This is consistent with the absence of a difference between the spectra of the S_p labels with the dT_8 and dU_8 duplexes (Figure 2).

In the following text, only the MD data for the R_p labels are further analyzed to explore the physical basis for the two key features observed in the EPR spectra: (i) difference between R_p -R5a- dT_8 and R_p -R5a- dU_8 ; and (ii) the lack of a detectable difference between R_p -R5- dT_8 and R_p -R5- dU_8 .

R_p -R5a and R_p -R5 show different t_2 and t_3 rotational behavior

Representative traces for torsion angles t_1 , t_2 and t_3 for R_p -R5a- dT_8 and R_p -R5- dT_8 are shown in Figure 4. A clear feature of R_p -R5a- dT_8 is that motions at t_2 and t_3 are limited on the nanosecond timescale. Throughout all simulations, including the one with the nitroxide starting conformation deliberately set at $t_2 = 120^\circ$, t_2 was fixed in the *trans* (t) conformation (Figure 4B, Tables 1 and S2). In comparison, t_2 for R_p -R5- dT_8 also favors a t conformation (Figure 4E, Tables 1 and S2), but deviations from t occur on the nanosecond timescale. Clearly the Br atom in R5a is restricting this motion.

For t_3 , the trace of R_p -R5a- dT_8 in Figure 4C shows persistence of a conformation around $+100^\circ$. However, analysis of all data for R_p -R5a- dT_8 (Tables 1 and S2) shows that t_3 adopts two conformations centered around $+100^\circ$ and -100° ($+260^\circ$), respectively, with infrequent transitions between these two positions. Among the eight 10-ns R_p -R5a- dT_8 simulations, 4 had no formal t_3 transition, and 4 gave only one transition (data not shown). In these two conformations, the pyrroline ring of R5a is positioned at the same location, but the peripheral functional groups (i.e., 4-Br, C2 and C5 methyls) are oriented differently with respect to the DNA. Over all R_p -R5a- dT_8 simulations, occupancy of the two t_3 conformations is approximately equal (Table 1). Similar $+100^\circ$ and -100° conformations are seen for R_p -R5- dT_8 , but with more frequent transitions between them (Figure 4F). The additional motion may reflect the greater mobility of t_2 , although there is no clear correlation between the t_2 and t_3 torsional angles for R_p -R5- dT_8 (Figure 4E, F).

The characteristics of t_2 and t_3 described for R5 and R5a occurred in all simulations regardless of diastereomeric configuration (R_p and S_p) and DNA sequence (dT_8 and dU_8) (Table 1). Therefore, they appear to be inherent properties of the respective labels. The MD results show that the presence of the 4-Br group limits rotations about bonds connecting the pyrroline ring to the DNA. The t_2 and t_3 motions in R_p -labels are similar for the dT_8 and dU_8 duplexes (Table 1), but limitations on t_2 and t_3 reduce the available conformations of R_p -R5a. This is an important factor in accounting for the sequence-dependent EPR spectral changes observed for R_p -R5a, but not for R_p -R5 (see below).

Interactions between R_p-R5a and DNA account for sequence-dependent changes in EPR spectra

For R_p-R5a, the t1 torsion samples the canonical *g*⁺, *t*, and *g*⁻ conformations (Figure 4A), with the dT₈ to dU₈ change significantly decreasing the t1 *g*⁺ occupancy (Table 1). Examples of R_p-R5a-dT₈ t1 *g*⁺ conformations with t3 = +100° or -100° are shown in Figures 5A and 5B, respectively. In both conformations, the nitroxide pyrroline ring is proximal to the dT₈ C5-methyl group in a face-on position, suggesting a direct interaction between these two entities. We also note that in Figures 5A and 5B the dG₆-pSdC₇ dinucleotide linkage adopts a B_{II} conformation (defined as ε/ζ: *g*⁻/*t*; e-ζ ~ +90°),³⁴ whereas all simulations started with dG₆-pSdC₇ in a B_I conformation (ε/ζ: *t*/*g*⁻; e-ζ ~ -90°).³⁴ The relationship between the nitroxide t1 torsion and dG₆-pSdC₇ dinucleotide conformation will be further examined later.

The characteristics of the conformers shown in Figures 5A and 5B are maintained for the entire R_p-R5a-dT₈ t1 *g*⁺ ensemble. Specifically, distributions of distances between the dT₈ C5-methyl group and center of the pyrroline ring, the peripheral methyl groups of the ring, and the 4-Br atom each show predominantly one population, with an average distance of 5.1 Å in each case (Table 2). These close contacts suggest the presence of a hydrophobic interaction between the label and the dT₈ C5-methyl group, which may explain the higher t1 *g*⁺ occupancy for R_p-R5a-dT₈ compared to R_p-R5a-dU₈.

The t1 *g*⁻ is another significantly occupied conformer for R_p-R5a (Table 1, Figure 5C). In this conformer, the pyrroline ring is moved away from the dT₈ C5-methyl group (compare Figures 5A and 5C), with the average distance between the center of the pyrroline ring and dT₈ C5-methyl becoming 6-8 Å (Table 2). At the same time, an average distance of <5.0 Å from the dT₈ C5-methyl to the R5a peripheral methyl groups or 4-Br atom is observed in three of the four ensembles of t1 *g*⁻ conformers (Table 2), as well as in one of the subpopulations of the fourth ensemble (*g*⁻,*t*, -100; B_{II}) (Table S4). This indicates that R_p-R5a t1 *g*⁻ conformers may also support interactions between the label and dT₈ C5-methyl. A similar conclusion can be drawn regarding the t1 *t* conformers (Table S4).

Overall, upon analysis of all R_p-R5a-dT₈ MD simulations, 86.8% of the conformer population was found to have one or more contacts of <5.0 Å between the dT₈ C5-methyl group and the center of the R_p-R5a pyrroline, a ring methyl group, or the 4-Br atom. This suggests that a majority of the population may support direct interaction between the dT₈ C5-methyl group and R_p-R5a. The dT₈ to dU₈ change abolishes this specific label/DNA interaction, thus resulting in the mobility changes observed in the EPR spectra of R_p-R5a-dT₈ and R_p-R5a-dU₈ (Figures 2 and 3).

Analysis of R_p-R5 sequence-dependent behavior

MD data reveal both similarities and differences between R_p-R5 and R_p-R5a. All major conformers of R_p-R5a are also present for R_p-R5 and maintain similar characteristics, as judged by the distances from the dT₈ C5-methyl to the pyrroline ring center and methyl groups (Tables 2, S4 and S5). This suggests that interaction between the label and dT₈ C5-methyl may occur for certain R_p-R5 conformers (e.g., t1 *g*⁺). However, contrary to R5a, R5 shows frequent transitions between t3 +100° and -100° (Figure 4F), as well as t2 transitions among *g*⁺, *t*, and *g*⁻ (Figure 4E). Consequently, R_p-R5 can access many more sterically allowed conformations compared to R_p-R5a, and many of them may not have interactions between dT₈ C5-methyl and the label (Tables 2 and S5). For example, in (t1 *g*⁻; t2 *g*⁻) conformers, which are largely absent in R_p-R5a but account for ~ 18% of the total R_p-R5 population (Table 2), the pyrroline ring center and methyl groups are on average >7.5 Å away from dT₈ C5-methyl (Table 2). These conformers are unlikely to be involved in direct

interactions between the label and the DNA. Furthermore, instead of a 4-Br atom, R5 has a 4-H (Figure 1A), which is unable to interact with dT₈ C5-methyl.

Overall, analyses of all R_p-R5-dT₈ MD simulations reveal that 40.1% of the label conformers have at least one distance <5.0 Å from the dT₈ C5-methyl group to the pyrroline ring center or a ring methyl group. This is more than a two-fold reduction compared to R_p-R5a. Therefore, it is likely that R_p-R5 shows no detectable sequence-dependent spectral changes because its sensitivity to the presence of the dT₈ C5-methyl is reduced by a combination of two factors: (i) fewer label functional groups making direct interactions with dT₈ C5-methyl; and (ii) a smaller fraction of conformers that include these interactions. Both of these changes originate from removal of the 4-Br atom.

Correlation of t1 and DNA backbone conformations for R_p labels

An intriguing feature observed for R_p labels was the apparent dependence of the t1 value on the DNA backbone conformation at the dG₆-pSdC₇ dinucleotide (Figure 5 and Table 2). This behavior is further illustrated in Figure 6 using one of the R_p-R5a-dT₈ simulations (simulation #27, Table S2). The t1 torsion angle shows a similar distribution to that in Figure 4A, with approximately half occupancy of *g*⁺ and *g*⁻ conformations (420° and 300°, respectively, in Figure 6A). Notably, the t1 *g*⁺ can only form when dG₆-pSdC₇ adopts a B_{II} conformation (Figure 6B, C). The strict association of t1 *g*⁺ with dG₆-pSdC₇ B_{II} is true for both R_p-R5a and R_p-R5, since the total occupancies of t1 *g*⁺; dG₆-pSdC₇ B_I for R_p-R5a-dT₈ and R_p-R5-dT₈ were only 0.02% and 0.07%, respectively, over all simulations (Tables 2, S4 and S5, Figure S1). Modeling showed that for a R_p label, the t1 *g*⁺ conformer has severe clashes of the pyrroline ring with the dG₆ sugar when dG₆-pSdC₇ remains in the B_I conformation, thus explaining the necessity of adopting the B_{II} conformation.

A control 30-ns MD simulation of the unlabeled dT₈ duplex gave a 35.3%:63.7% ratio for the B_I:B_{II} equilibrium at dG₆-dC₇ (Table S6, Figure S2). A similar B_I:B_{II} ratio was found upon analyzing all R_p-R5a-dT₈ and R_p-R5-dT₈ simulations (38.0%:61.8% and 40.9%:58.3%, respectively, Table S6). This suggests that interactions between the R_p labels and DNA are not strong enough to alter the thermodynamics of the B_I:B_{II} equilibrium. In addition, analysis of R_p-R5a-dU₈ traces shows approximately 52% B_{II} occupancy, indicating the nucleotide at position 8 does not significantly influence B_I/B_{II} equilibrium at dG₆-pSdC₇. Close examination of the MD traces show that the t1 *g*⁺ conformation does not induce the dG₆-pSdC₇ B_{II} conformation, but rather forms after a B_I to B_{II} transition at dG₆-pSdC₇. For example, the t1 *g*⁻ to *g*⁺ transition between 3 and 4 ns in Figure 6A clearly occurs after a B_I to B_{II} transition at dG₆-pSdC₇ (Figure 6B,C), and the intermediate structure (i.e., t1 *g*⁻; dG₆pSdC₇ B_{II}) is formed (Figure 5D).

Previously, MD simulations have observed B_I/B_{II} transitions occur in nanosecond timescale.³⁴⁻³⁷ Both MD simulation³⁶ and NMR measurements³⁷ have shown that a G_pC dinucleotide step, at which the R5/R5a labels were attached in this study, have a significant population of the B_{II} conformation. Overall, our results indicate that the R_p labels are exploring a naturally occurring transition of the DNA backbone to establish (additional) contact(s) between dT₈ C5-methyl group and the pyrroline ring, which subsequently influences nitroxide motions and gives rise to the observed cw-EPR spectral changes. This suggests a direct connection between label motion and local DNA backbone dynamics.

Discussion

A synergistic combination of EPR and MD simulation for probing DNA local environment using spin labeling

In this work, the behavior of R5 and R5a nitroxide labels in response to a subtle DNA sequence change was examined using a combination of EPR spectroscopy and MD simulation. X-band cw-EPR spectra of labeled DNA duplexes revealed that a dT₈ to dU₈ change altered the nanosecond rotational motions of R_p-R5a, but produced no detectable changes for S_p-R5a, R_p-R5, and S_p-R5. MD simulations suggested that hydrophobic interactions of the label with the dT₈ C5-methyl group and variations in the occupancy of label conformers that form these interactions, which account qualitatively for the observed EPR spectral changes. This demonstrates a synergistic interplay of experimental and computational approaches, with EPR measurements providing a critical validation of MD simulations, and the MD simulations revealing the molecular characteristics of the system and directing further experimental investigations (e.g., sequence changes). We note that in addition to the R5/R5a probes, a number of nitroxides have been reported to produce variable cw-EPR spectra depending on sequence and secondary structure of DNA and RNA.³⁸⁻⁴⁵ However, to connect the observed spectral features to molecular details at the nitroxide attachment site has been challenging. While MD simulations have been applied to investigate spin-labeled biomolecules,^{30,46-56} the combined EPR-mutagenesis-MD approach reported here could broadly aid further development and application of SDSL.

The results reported here also revealed issues that remain to be addressed in investigations of interactions between nitroxide labels and DNA. Specifically, force-field issues and ergodicity are always of concern in MD simulations. The force-field parameters used here have previously given results consistent with experimentally measured inter-nitroxide distances,³⁰ and the label parameters have also been used independently by other groups.^{55,56} However, there were relatively large variations in torsion angle distributions between the 10-ns traces (Tables 1, S2 and S3), indicating that convergence may not have been established. This hampers in-depth analyses, such as computing transition rates between label conformers and order parameters for a given ensemble, which are required for quantitative correlations with cw-EPR spectra. We note that new parameter sets for similar spin labels^{57,58} and improved DNA parameterizations^{36,59} have been proposed, particularly for longer (microsecond) simulations, and work has been reported on generating a full EPR spectrum based on MD trajectories, particularly taking advantage of advances in simulation techniques.⁴⁶⁻⁵¹ Thus, further improvement and extension of MD simulations may ultimately allow computation of R5/R5a spectra for direct comparison with experimental data.

Modulation of R5a/R5 motions by DNA

It has been hypothesized that site- and stereospecific behavior of R5 and R5a mainly arise from DNA sequence-dependent variations of (i) sterically allowable rotamer space; (ii) contacts/interactions between DNA and the pyrroline ring; and (iii) local DNA dynamics (flexibility).^{21,22} The results reported here provided details to validate this proposed framework, as well as revealing further complexity.

Regarding sterically allowable rotamers, MD simulations clearly demonstrated that steric exclusion from the DNA is a dominant factor that dictates the label behavior. For example, for R_p-R5, while *g*⁺, *t*, and *g*⁻ conformations are accessible to both t1 and t2, certain t1, t2 combinations (for example, *g*⁺, *g*⁺; *g*⁺, *g*⁻; and *g*⁻, *g*⁺) have <1% occupancy (Table S5), since they position the pyrroline ring within the steric volume of the DNA. In addition, when the DNA backbone at dG₆-pSdC₇ adopts a B₁ conformation, the t1 *g*⁺ conformer is hardly

occupied for R_p -R5a or R_p -R5 (Tables 2, S4, and S5, Figure S1) because of severe clashes between the pyrroline ring and the dG₆ sugar.

In terms of contacts/interactions between DNA and the pyrroline ring, simulations reveal that certain conformers of R_p labels (e.g., t1 g^+) position the dT₈ C5-methyl group within close proximity to the pyrroline ring and ring methyl groups, indicating probable hydrophobic contacts. For R_p -R5a, the 4-Br atom may further strengthen this label/DNA interaction, while at the same time increasing the fraction of these interaction-capable conformers by reducing the total number of allowed label conformers (Tables 2 and S4). This qualitatively accounts for the spectral differences between R_p -R5a-dT₈ and R_p -R5a-dU₈ (Figures 2 and 3). On the other hand, the absence of 4-Br in R_p -R5 reduces the percentage of interaction-enabled conformers and eliminates interactions between the DNA and the label C4 functionality (Tables 2 and S5), resulting in a lack of detectable spectral changes between R_p -R5-dT₈ and R_p -R5-dU₈ (Figure 2).

Last but not least, a connection between EPR detected R5/R5a motions to local nanosecond DNA backbone dynamics is demonstrated by the covariation of the dG₆-pSdC₇ B_I and R5/R5a t1 g^+ conformations (Table 2, Figures 6 and S1). In previous studies, B_I to B_{II} transitions in DNA duplexes have been reported to occur on a nanosecond timescale in a sequence-dependent manner, with the dG-dC dinucleotide step favoring substantial occupancy of the B_{II} conformation.³⁴⁻³⁷ The naturally-occurring nanosecond B_I/B_{II} transition at dG₆-pSdC₇ results in expanded sterically allowable rotamer space for the labels, allowing additional DNA-nitroxide contacts that influence nitroxide motions to an extent detectable by cw-EPR (i.e., R_p -R5a-dT₈ vs. R_p -R5-dU₈). In future studies, it should be very interesting to examine effects on R5/R5a motions from other modes of DNA motions (e.g., sugar puckering, base breathing).

Implications for use of R5a/R5 to probe dynamics and conformations of nucleic acids

Understanding of sequence-dependent coupling between DNA and R5/R5a will significantly improve our ability to extract information from these probes. For instance, spectral sensitivity of R_p -R5a to the dT->dU mutation may be further explored to probe sequence-dependent B_I/B_{II} transition, which may play a role in protein/DNA recognition.^{37,60-63} Interestingly, NMR³⁷ and MD³⁶ studies on B_I/B_{II} distributions for all 16 dinucleotide steps have revealed an asymmetric preference for B_{II} within dinucleotide base-pair units (e.g., a difference between G_pA and T_pC³⁷). These findings draw a parallel with asymmetric R5a/R5 EPR lineshapes previously obtained within dinucleotide base-pair units.^{21,22} This provides additional support to a link between DNA local backbone motion and R5a/R5 behavior.

Information on coupling between DNA and R5/R5a will also improve modeling of allowable nitroxide conformers and enable more accurate interpretation of inter-nitroxide distances. We have developed an algorithm, referred to as NASNOX,^{19,30} for rapid computation of distances between labels at two nucleotides in a DNA²⁰ or RNA structure.²³ This algorithm depends on prediction of the conformational distribution of each label. From a computational perspective, MD simulations demand significant computer resources and are difficult to apply for direct computation of multiple sets of inter-label distances.³⁰ Therefore, we envision a strategy in which the details of the label conformational distribution obtained from MD simulations of model systems are incorporated empirically in a simple conformer search model, thus enabling efficient and accurate calculations of inter-label distances in the context of determination of nucleic acid folds.

We note that computational approaches, including MD simulations, have been an important tool in characterizing sequence-dependent conformational and dynamic heterogeneity of free

DNA duplexes,^{36,64-67} but experimental validation of conclusions drawn from these analyses remains challenging. The combined experimental (EPR spectroscopy, DNA mutagenesis) and computational (MD simulations) approach reported in this work paves the way for an in-depth understanding of the behavior of R5a/R5 at a given DNA micro-environment. This is a key step forward towards the use of R5a/R5 to examine intrinsic sequence-dependent conformational and dynamic heterogeneity in large biologically relevant DNA molecules under physiological conditions.

Supplementary Material

Refer to Web version on PubMed Central for supplementary material.

Acknowledgments

We gratefully acknowledge support from NIH (GM069557, PZQ), NSF (MCB 054652, PZQ) and a fellowship from Hashemite University (Jordan) to MH. We thank Dr. Kálmán Hideg (University of Pécs, Pécs, Hungary) for providing reactive precursors of the R5 and R5a probes. Computation for the work described in this paper was supported by the University of Southern California Center for High-Performance Computing and Communications (www.usc.edu/hpcc).

References

1. Lawson, CL.; Berman, HM. Indirect Readout of DNA Sequence by Proteins. In: Correll, CC.; Rice, PA., editors. Protein-Nucleic Acid Interactions. Royal Society of Chemistry; Cambridge: 2008. p. 66
2. Rohs R, West SM, Liu P, Honig B. *Curr Opin Struct Biol.* 2009; 19:171. [PubMed: 19362815]
3. Rohs R, Jin X, West SM, Joshi R, Honig B, Mann RS. *Annu Rev Biochem.* 2010; 79:233. [PubMed: 20334529]
4. Egli M, Pallan PS. *Curr Opin Struct Biol.* 2010; 20:262. [PubMed: 20381338]
5. Segal E, Fondufe-Mittendorf Y, Chen L, Thastrom A, Field Y, Moore IK, Wang JP, Widom J. *J Nature.* 2006; 442:772.
6. Peckham HE, Thurman RE, Fu Y, Stamatoyannopoulos JA, Noble WS, Struhl K, Weng Z. *Genome Res.* 2007; 17:1170. [PubMed: 17620451]
7. Rohs R, West SM, Sosinsky A, Liu P, Mann RS, Honig B. *Nature.* 2009; 461:1248. [PubMed: 19865164]
8. Hubbell WL, Cafiso DS, Altenbach C. *Nat Struct Biol.* 2000; 7:735. [PubMed: 10966640]
9. Fajer, PG. Electron spin resonance spectroscopy labeling in proteins and peptides analysis. In: Meyers, R., editor. *Encyclopedia of analytical chemistry.* John Wiley & Sons; Chichester: 2000. p. 5725
10. Klug CS, Feix JB. *Methods Cell Biol.* 2008; 84:617. [PubMed: 17964945]
11. Sowa GZ, Qin PZ. Site-directed spin labeling studies on nucleic acid structure and dynamics. *Prog Nucleic Acids Res Mol Biol.* 2008; 82:147.
12. Robinson BH, Mailer C, Drobny G. *Annu Rev Biophys Biomol Struct.* 1997; 26:629. [PubMed: 9241432]
13. Keyes, RS.; Bobst, AM. Spin-labeled nucleic acids. In: Berliner, LJ., editor. *Biological Magnetic Resonance.* Vol. 14. Plenum Press; New York: 1998. p. 283
14. Krsti , I.; Endeward, B.; Margraf, D.; Marko, A.; Prisner, T. Structure and Dynamics of Nucleic Acids. In: Drescher, M.; Jeschke, G., editors. *EPR Spectroscopy, Applications in Chemistry and Biology.* Vol. 321. Springer; Berlin / Heidelberg: 2011. p. 159
15. Reginsson GW, Schiemann O. *Biochem Soc Trans.* 2011; 39:128. [PubMed: 21265760]
16. Sigurdsson ST. *Pure Appl Chem.* 2011; 83:677.
17. Nguyen P, Qin PZ. *WIREs: RNA.* 2012; 3:62. [PubMed: 21882345]
18. Qin PZ, Butcher SE, Feigon J, Hubbell WL. *Biochemistry.* 2001; 40:6929. [PubMed: 11389608]

19. Qin PZ, Haworth IS, Cai Q, Kusnetzow AK, Grant GPG, Price EA, Sowa GZ, Popova A, Herreros B, He H. *Nat Protocols*. 2007; 2:2354.
20. Cai Q, Kusnetzow AK, Hubbell WL, Haworth IS, Gacho GPC, Van Eps N, Hideg K, Chambers EJ, Qin PZ. *Nucleic Acids Res*. 2006; 34:4722. [PubMed: 16966338]
21. Popova AM, Kálai T, Hideg K, Qin PZ. *Biochemistry*. 2009; 48:8540. [PubMed: 19650666]
22. Popova AM, Qin PZ. *Biophys J*. 2010; 99:2180. [PubMed: 20923652]
23. Cai Q, Kusnetzow AK, Hideg K, Price EA, Haworth IS, Qin PZ. *Biophys J*. 2007; 93:2110. [PubMed: 17526583]
24. Grant GPG, Boyd N, Herschlag D, Qin PZ. *J Am Chem Soc*. 2009; 131:3136. [PubMed: 19220053]
25. Zhang X, Tung C-S, Sowa GZ, Hatmal MM, Haworth IS, Qin PZ. *J Am Chem Soc*. 2012; 134:2644. [PubMed: 22229766]
26. Grant GPG, Popova A, Qin PZ. *Biochem Biophys Res Commun*. 2008; 371:451. [PubMed: 18442474]
27. Earle, KA.; Budil, DE. Calculating Slow-motion ESR Spectra of Spin-Labeled Polymers. In: Schlick, S., editor. *Advanced ESR Methods in Polymer Research*. John Wiley and Sons; New York: 2006. p. 53
28. Meirovitch E, Nayeem A, Freed JH. *J Phys Chem B*. 1984; 88:3454.
29. Leporc S, Mauffret O, Tevanian G, Lescot E, Monnot M, Femandjian S. *Nucleic Acids Res*. 1999; 27:4759. [PubMed: 10572176]
30. Price EA, Sutch BT, Cai Q, Qin PZ, Haworth IS. *Biopolymers*. 2007; 87:40. [PubMed: 17538992]
31. Wang J, Wolf RM, Caldwell JW, Kollman PA, Case DA. *J Comput Chem*. 2004; 25:1157. [PubMed: 15116359]
32. Darden T, York D, Pedersen L. *J Chem Phys*. 1993; 98:10089.
33. Lavery R, Sklenar H. *J Biomol Struct Dyn*. 1988; 6:63. [PubMed: 2482765]
34. Hartmann B, Piazzola D, Lavery R. *Nucleic Acids Res*. 1993; 21:561. [PubMed: 8441668]
35. Perez A, Luque FJ, Orozco M. *J Am Chem Soc*. 2007; 129:14739. [PubMed: 17985896]
36. Lavery R, Zakrzewska K, Beveridge D, Bishop TC, Case DA, Cheatham T 3rd, Dixit S, Jayaram B, Lankas F, Lughton C, Maddocks JH, Michon A, Osman R, Orozco M, Perez A, Singh T, Spackova N, Sponer J. *Nucleic Acids Res*. 2010; 38:299. [PubMed: 19850719]
37. Heddi B, Oguey C, Lavelle C, Foloppe N, Hartmann B. *Nucleic Acids Res*. 2010; 38:1034. [PubMed: 19920127]
38. Okonogi TM, Alley SC, Reese AW, Hopkins PB, Robinson BH. *Biophys J*. 2000; 78:2560. [PubMed: 10777752]
39. Edwards TE, Okonogi TM, Robinson BH, Sigurdsson ST. *J Am Chem Soc*. 2001; 123:1527. [PubMed: 11456739]
40. Gannett PM, Darian E, Powell J, Johnson EM, Mundoma C, Greenbaum NL, Ramsey CM, Dalal NS, Budil DE. *Nucleic Acids Res*. 2002; 30:5328. [PubMed: 12466559]
41. Cekan P, Jonsson EO, Sigurdsson ST. *Nucleic Acids Res*. 2009; 37:3990. [PubMed: 19406921]
42. Cekan P, Sigurdsson ST. *J Am Chem Soc*. 2009; 131:18054. [PubMed: 19928915]
43. Smith AL, Cekan P, Brewood GP, Okonogi TM, Alemayehu S, Hustedt EJ, Benight AS, Sigurdsson ST, Robinson BH. *J Phys Chem B*. 2009; 113:2664. [PubMed: 19708106]
44. Krstic I, Frolow O, Sezer D, Endeward B, Weigand JE, Suess B, Engels JW, Prisner TF. *J Am Chem Soc*. 2010; 132:1454. [PubMed: 20078041]
45. Shelke SA, Sigurdsson ST. *Nucleic Acids Res*. 2011
46. Robinson BH, Slusky LJ, Auteri FP. *J Chem Phys*. 1992; 96:2609.
47. Stoica I. *J Phys Chem B*. 2003; 108:1771.
48. Beier C, Steinhoff H-J. *Biophys J*. 2006; 91:2647. [PubMed: 16844740]
49. Budil DE, Sale KL, Khairy KA, Fajer PG. *J Phys Chem A*. 2006; 110:3703. [PubMed: 16526654]
50. DeSensi SC, Rangel DP, Beth AH, Lybrand TP, Hustedt EJ. *Biophys J*. 2008; 94:3798. [PubMed: 18234808]
51. Sezer D, Freed JH, Roux B. *J Am Chem Soc*. 2009; 131:2597. [PubMed: 19191603]

52. Sale K, Song L, Liu YS, Perozo E, Fajer P. *J Am Chem Soc.* 2005; 127:9334. [PubMed: 15984837]
53. Fajer MI, Li H, Yang W, Fajer PG. *J Am Chem Soc.* 2007; 129:13840. [PubMed: 17948993]
54. Piton N, Mu Y, Stock G, Prisner TF, Schiemann O, Engels JW. *Nucl Acids Res.* 2007; 35:3128. [PubMed: 17452362]
55. Ding F, Layten M, Simmerling C. *J Am Chem Soc.* 2008; 130:7184. [PubMed: 18479129]
56. Galiano L, Ding F, Veloro AM, Blackburn ME, Simmerling C, Fanucci GE. *J Am Chem Soc.* 2009; 131:430. [PubMed: 19140783]
57. Houriez, Cl; Ferrei, N.; Siri, D.; Masella, M. *J Phys Chem B.* 2009; 113:15047. [PubMed: 19845322]
58. Stendardo E, Pedone A, Cimino P, Cristina Menziani M, Crescenzi O, Barone V. *Phys Chem Chem Phys.* 2010; 12:11697. [PubMed: 20714476]
59. Perez A, Marchan I, Svozil D, Sponer J, Cheatham TE 3rd, Laughton CA, Orozco M. *Biophys J.* 2007; 92:3817. [PubMed: 17351000]
60. Wecker K, Bonnet MC, Meurs EF, Delepierre M. *Nucleic Acids Res.* 2002; 30:4452. [PubMed: 12384592]
61. Heddi B, Foloppe N, Bouchemal N, Hantz E, Hartmann B. *J Am Chem Soc.* 2006; 128:9170. [PubMed: 16834390]
62. Rene B, Masliah G, Antri SE, Femandjian S, Mauffret O. *J Phys Chem B.* 2007; 111:4235. [PubMed: 17391020]
63. Tian Y, Kayatta M, Shultis K, Gonzalez A, Mueller LJ, Hatcher ME. *J Phys Chem B.* 2009; 113:2596. [PubMed: 18717548]
64. Olson WK, Gorin AA, Lu XJ, Hock LM, Zhurkin VB. *Proc Natl Acad Sci U S A.* 1998; 95:11163. [PubMed: 9736707]
65. Lankas F, Sponer J, Langowski J, Cheatham TE 3rd. *Biophys J.* 2003; 85:2872. [PubMed: 14581192]
66. Fujii S, Kono H, Takenaka S, Go N, Sarai A. *Nucleic Acids Res.* 2007; 35:6063. [PubMed: 17766249]
67. Goni JR, Perez A, Torrents D, Orozco M. *Genome Biol.* 2007; 8:R263. [PubMed: 18072969]

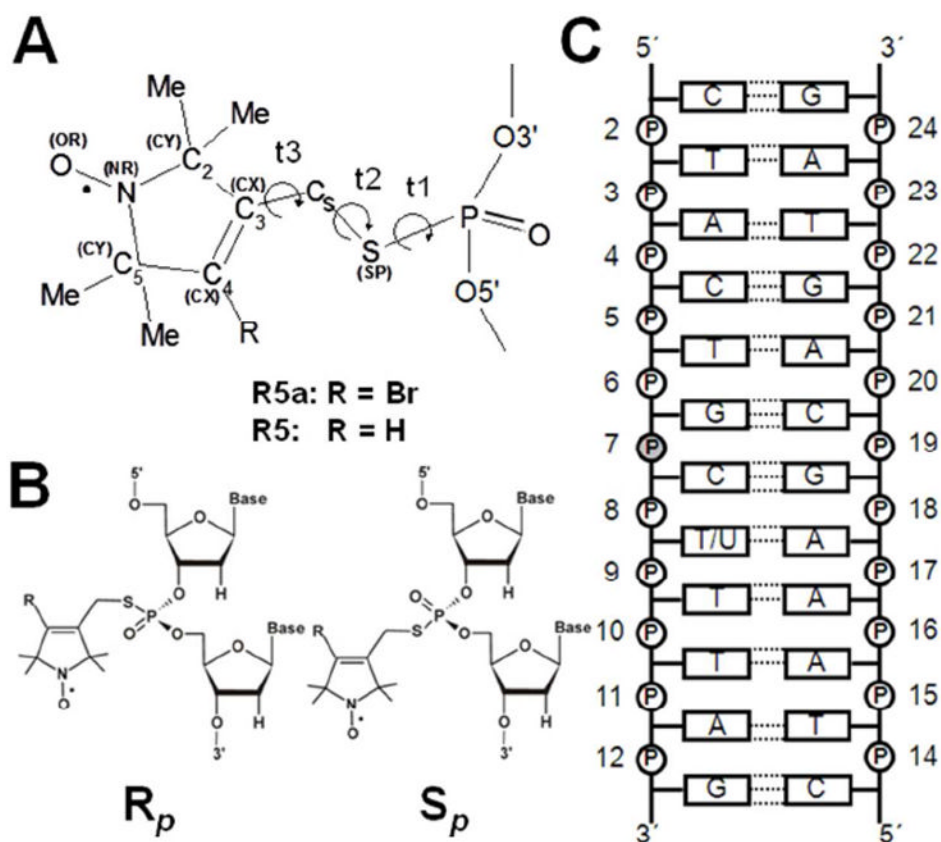


Figure 1.

(A) Structure of nitroxide labels (R5: R=H; R5a: R=Br). The torsional angles of the DNA-label linker are defined as t1 (O5'-P-S-C_s), t2 (P-S-C_s-C₃) and t3 (S-C_s-C₃-C₂). Symbols in parentheses indicate non-standard atom types³⁰ used in the AMBER force field. (B) Absolute R_p and S_p configurations of the labeled phosphorothioate. (C) DNA duplex used in the study. The phosphorothioate-substituted and labeled nucleotide (p_SC7) is shaded. Nucleotide 8 of the DNA was dT or dU. p_SC7 was labeled with R5a or R5 as the R_p or S_p diastereoisomer.

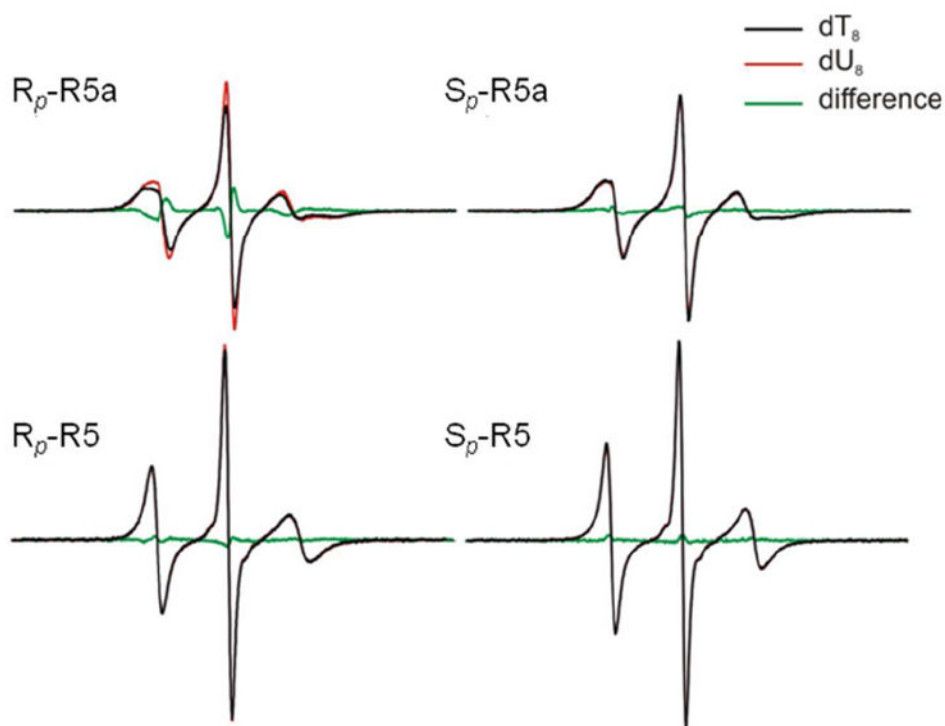


Figure 2. EPR spectra obtained at 25°C. Black lines represent spectra obtained in the $d(\text{CTACTG}_{pS}\text{C}_7\text{T}_8\text{TTAG})\cdot d(\text{CTAAAGCAGTAG})$ duplexes ($d\text{T}_8$), and red lines represent those in the $d(\text{CTACTG}_{pS}\text{C}_7\text{U}_8\text{TTAG})\cdot d(\text{CTAAAGCAGTAG})$ duplexes ($d\text{U}_8$). Green lines represent the corresponding difference spectra.

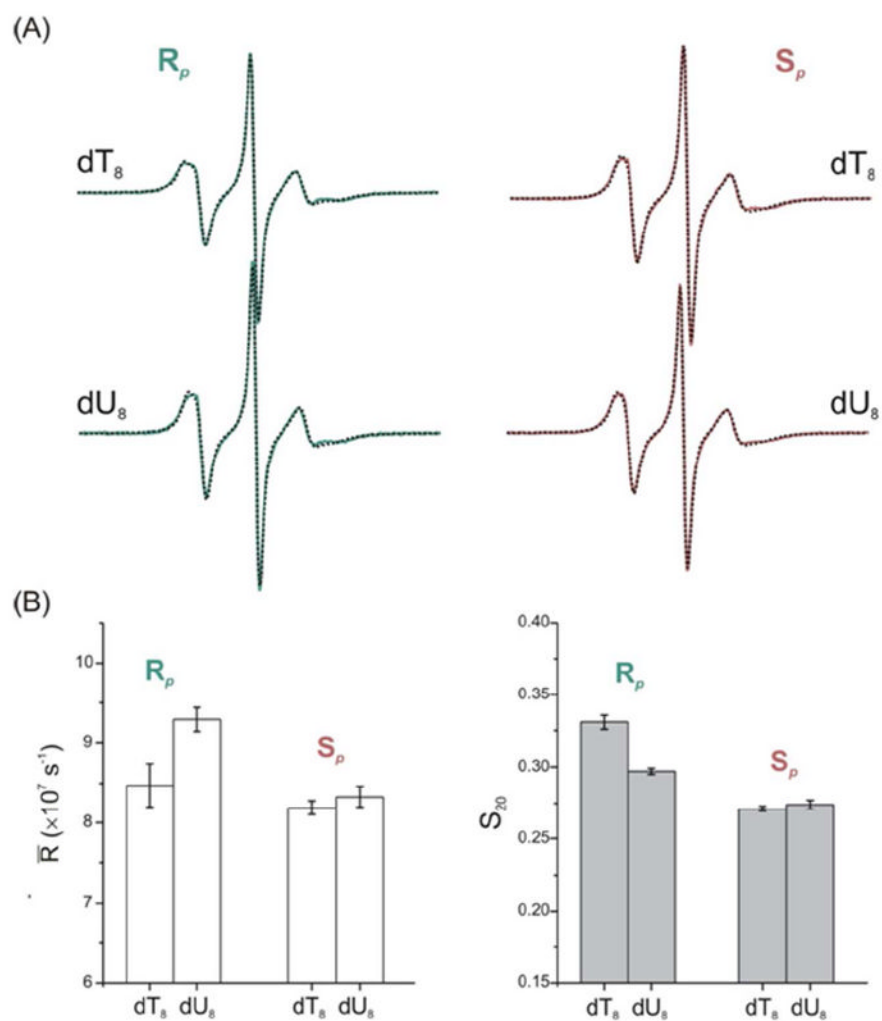
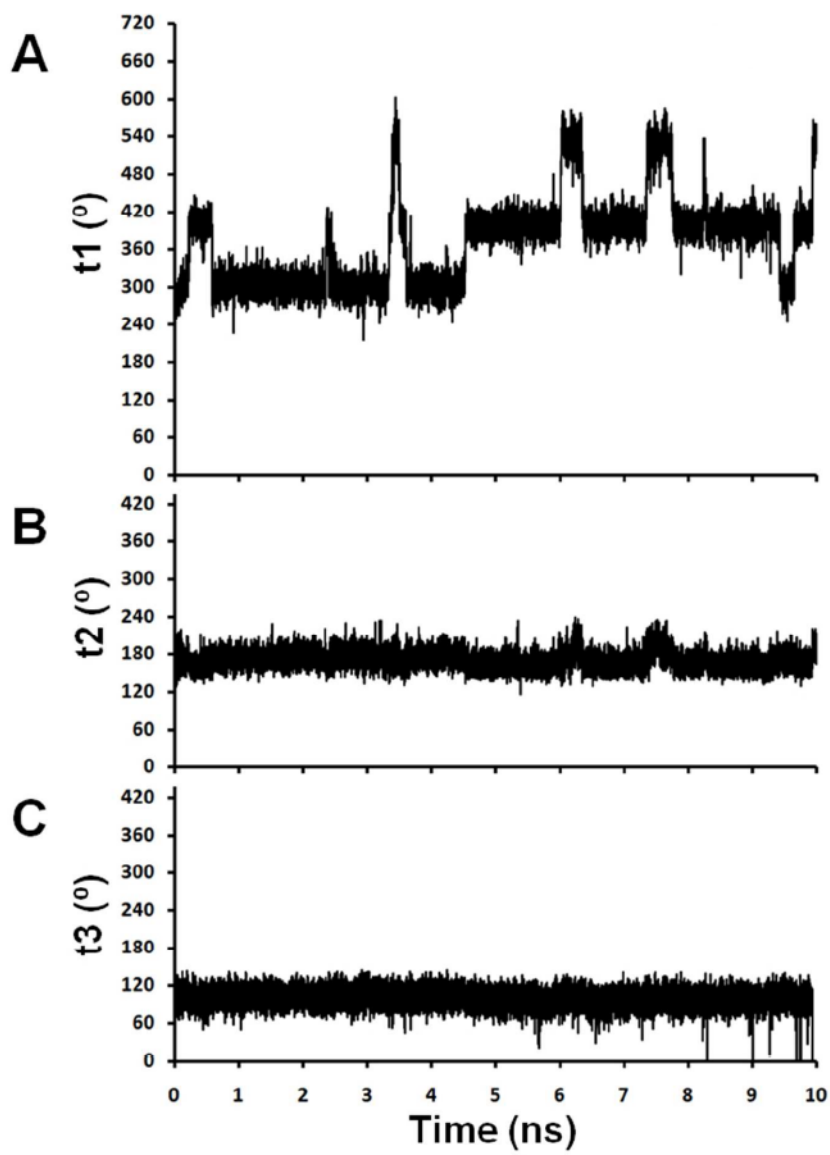


Figure 3. R5a spectral simulations. (A) Overlays of measured (solid lines) and simulated (dotted lines) spectra. (B) Comparisons of nitroxide motional parameters obtained from simulations. Additional details on simulation parameters are given in Table S1.



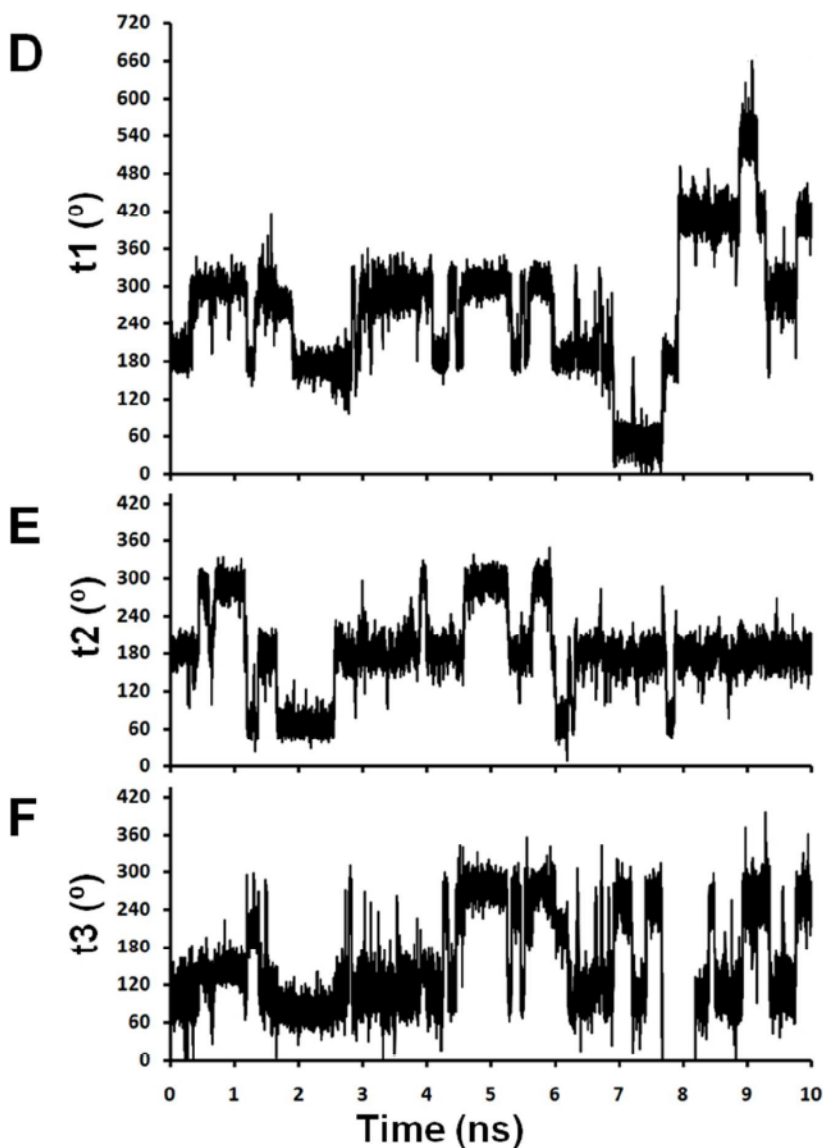


Figure 4. Sample traces of torsional motions for R_p -R5a-dT₈ (A, t₁; B, t₂; C, t₃; simulation #1) and R_p -R5-dT₈ (D, t₁; E, t₂; F, t₃; simulation #13). The t₁ traces (A, D) are shown over a range of 0-720° with occupancy of *g*⁺ (60° or 420°), *t* (180° or 540°), and *g*⁻ (300° or 660°). In F, the trace between 7.5 and 8.5 ns reflects t₃ motion from +260° through a 360° turn to -100° (an equivalent conformation with a numerical value off the scale of the y-axis) and then a reverse 360° turn back to +260°, with only brief occupancy of the +100° conformer during each full turn.

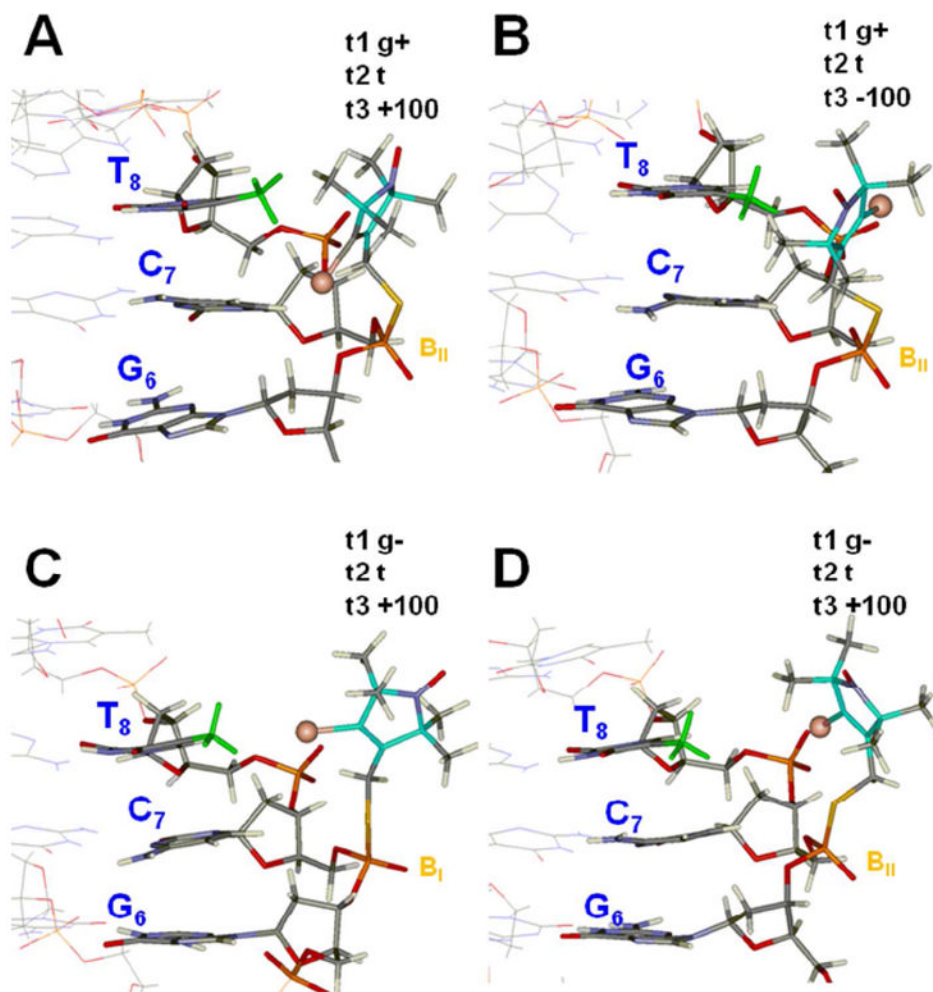


Figure 5. Representative structures from simulations of R_p -R5a-dT8. A. $t_1 g^+$, $t_2 t$, $t_3 +100^\circ$, dG₆-psdC₇ B_{II} (simulation #1, at 5 ns, see Fig. 4A-C). B. $t_1 g^+$, $t_2 t$, $t_3 -100^\circ$, dG₆-psdC₇ B_{II} (#37, at 8 ns). C. $t_1 g^-$, $t_2 t$, $t_3 +100^\circ$, dG₆-psdC₇ B_I (#1, at 2 ns, see Fig. 4A-C). D. $t_1 g^-$, $t_2 t$, $t_3 +100^\circ$, dG₆-psdC₇ B_{II} (#27, at 3.8 ns, see Fig. 6). In each structure, the dT₈ methyl group is colored green, the C atoms of the pyrroline ring are colored light blue, and the bromine atom is shown as a brown sphere. The backbone conformation for the dG₆-psdC₇ dinucleotide (B_I or B_{II}) is shown in orange.

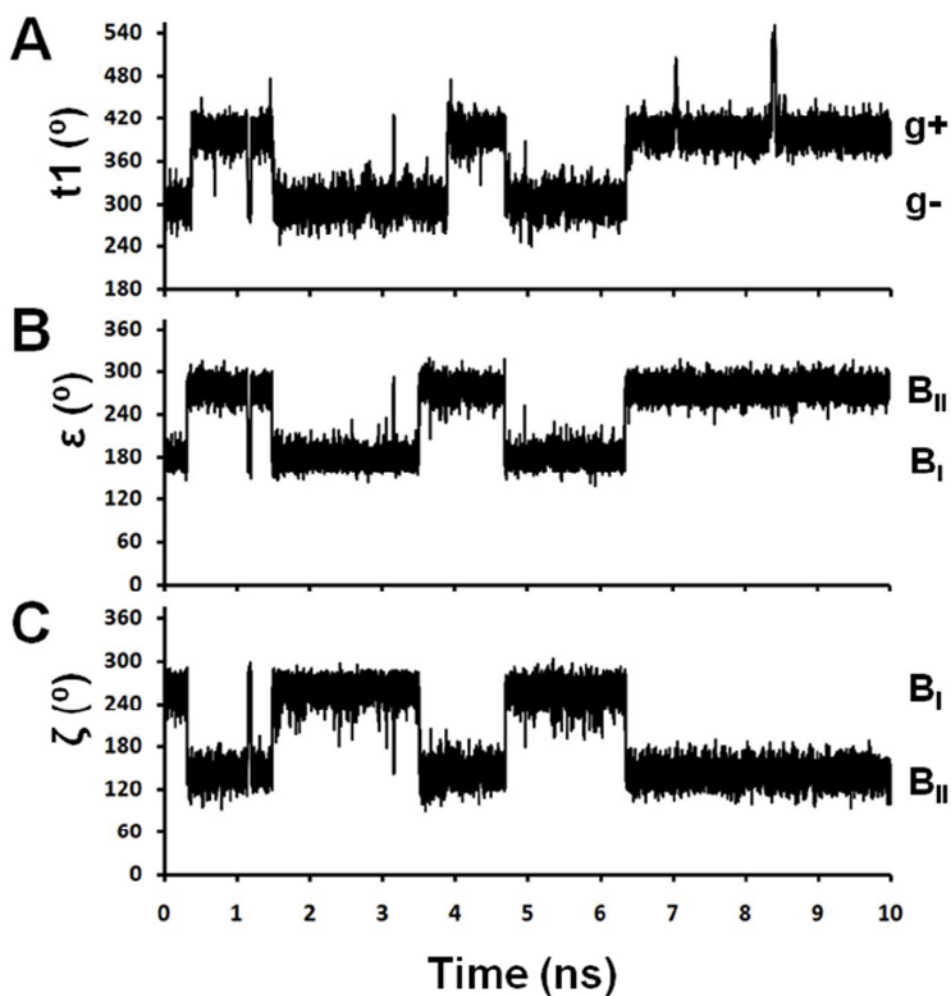


Figure 6. Sample traces of torsional motions for R_p -R5a-dT₈ (simulation #27). A. t_1 . B. ϵ torsion angle of dG₆: t conformers correspond to the B_I conformation at dG₆-pSdC₇ and g - conformers to B_{II}. C. ζ torsion angle of dG₆: g - conformers correspond to the B_I conformation and approximately t conformers to B_{II}. See Table S6 for detailed definition of B_I and B_{II} conformations.

Label conformer distributions in molecular dynamics simulations of DNA duplexes of sequence d(CTACTG_{pS}C₇Y₈TTAG).d(CTAAAAGCAGTAG) (Y = T or U) labeled with a 1-oxy-4-bromo-2,2,5,5-tetramethylpyrroline (R5a) or a 1-oxy-1,2,2,5,5-tetramethylpyrroline (R5) radical at pSdC₇.

Table 1

Label	Chirality	dY ₈	n ^a	t1 (%) ^{b,c}			t2 (%) ^{b,c}			t3 (%) ^{b,d}		
				g+	g-	t	g+	g-	t	g+	g-	-100°
R5a	R _p	dT ₈	8	46.6±24.3	11.6±13.5	41.8±27.7	0.5±0.7	98.9±2.3	0.6±1.8	64.4±39.6	35.6±39.6	
R5a	R _p	dU ₈	6	17.7±9.7	23.9±16.3	58.4±25.4	2.9±4.4	93.6±6.0	3.5±4.1	57.5±33.7	42.5±33.7	
R5	R _p	dT ₈	3	18.5±4.9	23.8±9.5	57.6±13.0	8.8±6.5	72.7±5.7	18.5±1.0	52.8±7.9	47.2±7.9	
R5	R _p	dU ₈	3	14.2±8.8	16.8±9.7	68.9±4.8	13.3±6.9	67.0±17.1	19.7±21.6	51.3±10.1	48.7±10.1	
R5a	S _p	dT ₈	8	48.6±9.7	48.7±9.3	2.6±1.4	5.8±4.7	88.7±8.2	5.5±7.0	69.1±35.8	31.1±35.9	
R5a	S _p	dU ₈	6	37.0±14.2	59.0±14.9	3.9±2.1	4.9±7.9	91.0±7.2	4.2±4.6	60.1±35.5	39.9±35.5	
R5	S _p	dT ₈	3	52.7±19.5	45.3±18.2	2.0±1.7	21.2±9.3	59.7±3.7	19.1±12.6	46.3±20.6	53.7±20.6	
R5	S _p	dU ₈	3	38.8±18.2	58.8±17.3	2.4±1.3	8.9±4.7	58.0±5.6	33.1±8.9	54.0±6.9	46.0±6.9	

^aNumber of simulations of 10 ns each.

^bTorsion angles are defined in Figure 1A. Average and standard deviations are calculated from the corresponding individual 10-ns simulations.

^cg+: 0-120°; t: 120-240°; g-: 240-360°

^dTorsion angle t3 adopts values centered on +100° and -100°. Each distribution was determined based on conformations with t3 > 0° and t3 < 0°, respectively, for a torsional angle range from +180° to -180°.

Table 2

Distances from the 5-methyl carbon atom of dT₈ to R_PR5a and R_PR5 labels in key conformers found in simulations of the labeled DNA duplex d(CTACTG_pS_CT₈TTAG).d(CTAAAAGCAGTAG).^a

Conformer ^b (t1,t2,t3)	DNA ^c	R5a	R5a ^d Occupancy (%)	R5a ^d Pyrroline ring center (Å)	R5a ^d Closest ring methyl (Å)	R5a ^d Ring 4-Br (Å)	R5	R5 ^d Occupancy (%)	R5 ^d Pyrroline ring center (Å)	R5 ^d Closest ring methyl (Å)
g+,t,+100	B _I	0.0 ^e	---	---	---	---	0.0 ^e	---	---	---
g+,t,-100	B _I	0.0 ^e	---	---	---	---	0.0 ^e	---	---	---
g+,t,+100	B _{II}	32.9	4.9 ± 0.5	4.1 ± 0.5	4.9 ± 0.9	8.8	8.8	5.4 ± 0.7	4.0 ± 0.5	
g+,t,-100	B _{II}	13.6	5.1 ± 0.7	4.3 ± 0.6	5.0 ± 1.2	9.2	9.2	5.3 ± 0.7	4.2 ± 0.6	
g-,t,+100	B _I	27.9	6.6 ± 0.8	5.8 ± 0.9	4.2 ± 0.5	9.6 ^f	9.6 ^f	6.9 ± 1.6	6.1 ± 1.9	
g-,t,-100	B _I	8.3	6.3 ± 0.8	4.1 ± 0.8	8.9 ± 0.7	16.1	16.1	6.4 ± 0.9	4.2 ± 1.0	
g-,t,+100	B _{II}	1.7	7.0 ± 0.8	6.4 ± 1.0	4.4 ± 0.8	6.6 ^f	6.6 ^f	8.4 ± 1.3	8.1 ± 1.5	
g-,t,-100	B _{II}	3.1 ^f	8.1 ± 1.4	6.0 ± 1.6	9.6 ± 1.1	5.0 ^f	5.0 ^f	7.7 ± 1.5	5.7 ± 1.7	
g-,g ₊ ,+100	B _I	0.0 ^e	---	---	---	---	2.8 ^f	8.9 ± 1.4	7.5 ± 1.6	
g-,g ₋ ,+100	B _I	0.2	9.3 ± 1.0	9.4 ± 1.2	7.8 ± 0.9	2.9 ^f	2.9 ^f	8.3 ± 1.3	8.1 ± 1.5	
g-,g ₊ ,+100	B _{II}	0.0 ^e	---	---	---	---	10.0	9.7 ± 0.7	9.1 ± 0.8	
g-,g ₋ ,+100	B _{II}	0.4	9.4 ± 0.8	9.0 ± 0.9	8.8 ± 0.8	2.5	2.5	9.4 ± 0.9	9.4 ± 1.0	

^a Analyses carried out on 400,000 R_PR5a-dT₈ structures (eight 10-ns simulations) and 150,000 R_PR5-dT₈ structures (three 10-ns simulations). Data for all conformers are shown in Tables S4 (R5a) and S5 (R5).

^b g₊: 0-120°; t: 120-240°; g₋: 240-360°

^c Backbone conformation at the dG₆pSdC₇ dinucleotide (see Table S6)

^d Average ± standard deviation of distance (Å) determined for the corresponding ensemble of conformers.

^e Occupancy ranges from 0% to 0.03% (see Tables S4 (R5a) and S5 (R5)).

^f Bimodal distributions observed (see Table S4 (R5a) and S5 (R5)).